Analysis of Flux-Split Algorithms for Euler's Equations with Real Gases

B. Grossman* and R. W. Walters†
Virginia Polytechnic Institute and State University, Blacksburg, Virginia

An analysis of flux-splitting procedures for the solution of Euler's equations with real gas effects is presented. An alternative real gas flux splitting is derived which can easily be implemented into existing codes. This approach, which takes the form of an "equivalent" γ representation is not an ad hoc model, but is based on theoretical considerations. Details of this method with the Steger-Warming and Van Leer flux-vector splittings and the Roe flux-difference splitting are given. Applications of the method to several high Mach number, high-temperature, equilibrium airflows are presented for one and two space dimensions.

Introduction

CURRENT emphasis on the hypersonic flight regime requires the development of computational procedures for flows with real gas effects. Many of the modern techniques of computational fluid dynamics have algorithms that fall into the category of "upwind" schemes.[1] These methods, which include flux-vector splitting and flux-difference splitting, utilize difference procedures that are biased in the direction determined by the signs of the characteristic speeds. These approaches generally have been developed for perfect gases, and the schemes do not directly extend to real gas flows. The objective of this paper is to examine the derivation of the upwind schemes of Steger-Warming,[2] Van Leer,[3] and Roe[4] within the context of real gas effects.

Colella and Glaz[5] have recently performed a detailed examination of real gas computational procedures. They have developed an approximate procedure based on a local parameterization of the equation of state and implemented the method into a second-order Godunov scheme.

The present work was influenced by the approach of Ref. 5, particularly the treatment of the equation of state. However, by examining the details of existing flux-splitting procedures, we have determined an alternative real gas flux splitting, which can be easily implemented into existing codes. This approach, which develops as an "equivalent" γ representation is not an ad hoc model, but is based on theoretical considerations. The details of our procedure are presented in the next section. Some preliminary computations for real gas flows in one and two space dimensions are then described. These calculations indicate the accuracy of the method and the ability of these procedures to be implemented into existing flux-vector split and flux-difference split, perfect gas codes.

Analysis

In order to develop our algorithms for real gas flows, we will first consider the one-dimensional Euler equations. We write the equations in vector conservation form as

$$\bar{Q}_t + \bar{F}_x = 0 \tag{1}$$

where

$$\bar{Q} = \begin{bmatrix} \rho \\ \rho u \\ \rho E \end{bmatrix}, \qquad \bar{F} = \begin{bmatrix} \rho u \\ \rho u^2 + p \\ (\rho E + p)u \end{bmatrix} \tag{2}$$

where ρ is the density, u is the velocity, with the total energy per unit mass $E = e + u^2/2$ and e being the internal energy per unit mass.

We assume that we have a general equation of state of the form

$$p = p(\tau, e) \tag{3}$$

where the specific volume $\tau = 1/\rho$. The speed of sound can then be determined as

$$a^2 = \left(\frac{\partial p}{\partial \rho}\right)_s = \tau^2(pp_e - p_\tau) \tag{4}$$

where the relationship $(\partial e/\partial \tau)_s = p$ stemming from the first law of thermodynamics has been utilized. The partial derivatives p_e and p_τ are $(\partial p/\partial e)_\tau$ and $(\partial p/\partial \tau)_e$ and are obtained, in principle, from Eq. (3).

The first step of developing a flux-vector splitting is to develop the Jacobian matrix $A = \partial \bar{F}/\partial \bar{Q}$. It is found that

$$A = \begin{bmatrix} 0 & 1 & 0 \\ -u^2 & 2u & 0 \\ -u\left(E + \frac{p}{\rho}\right) & E + \frac{p}{\rho} & u \end{bmatrix} - \frac{1}{\rho^2} p_\tau \begin{bmatrix} 0 & 0 & 0 \\ 1 & 0 & 0 \\ u & 0 & 0 \end{bmatrix}$$

$$- \frac{1}{\rho} p_e \begin{bmatrix} 0 & 0 & 0 \\ \left(e - \frac{u^2}{2}\right) & u & -1 \\ u\left(e - \frac{u^2}{2}\right) & u^2 & -u \end{bmatrix} \tag{5}$$

This form of the matrix A is not very enlightening, although it can be verified that the eigenvalues of A are $u \pm a$ and u

Received Sept. 28, 1987; revision received April 15, 1988.

*Professor, Department of Aerospace and Ocean Engineering. Member AIAA.

†Assistant Professor, Department of Aerospace and Ocean Engineering. Member AIAA.

with the speed of sound a defined by Eq. (4). A more interesting form is seen by examining the form of the derivatives p_e and p_τ for a perfect gas, where

$$p = (\gamma - 1)e/\tau$$

For our real gas, we can consider an equivalent $\tilde{\gamma}$ such that

$$p = (\tilde{\gamma} - 1)e/\tau \tag{6}$$

where obviously $\tilde{\gamma} = \tilde{\gamma}(e, \tau)$. We have not lost any generality in our real gas model, nor are we presupposing any behavior for $\tilde{\gamma}$. (However, as noted in Ref. 5, this function $\tilde{\gamma}$ will surely vary more slowly than other thermodynamic variables since for any values of e and τ, even those varying over several orders of magnitude, $\tilde{\gamma}$ will remain between 1 and 5/3.)

Replacing the p_τ and p_e derivatives in Eq. (5) with

$$p_\tau = -\frac{p}{\tau} + \frac{p}{\tilde{\gamma} - 1}\tilde{\gamma}_\tau$$

$$p_e = \frac{p}{e} + \frac{p}{\tilde{\gamma} - 1}\tilde{\gamma}_e$$

we obtain A as

$$A = \tilde{A} - \frac{e}{\rho}\tilde{\gamma}_\tau \begin{bmatrix} 0 & 0 & 0 \\ 1 & 0 & 0 \\ u & 0 & 0 \end{bmatrix} - e\tilde{\gamma}_e \begin{bmatrix} 0 & 0 & 0 \\ e - u^2/2 & u & -1 \\ u(e - u^2/2) & u^2 & -u \end{bmatrix} \tag{7}$$

where

$$\tilde{A} = \begin{bmatrix} 0 & 1 & 0 \\ (\tilde{\gamma} - 3)u^2/2 & (3 - \tilde{\gamma})u & \tilde{\gamma} - 1 \\ -\tilde{\gamma}ue + (\tilde{\gamma} - 2)u^3/2 & \tilde{\gamma}e + (3 - 2\tilde{\gamma})u^2/2 & \tilde{\gamma}u \end{bmatrix} \tag{8}$$

In this form we see that for a perfect gas where $\tilde{\gamma} = \gamma$ and $\tilde{\gamma}_\tau = 0$, $\tilde{\gamma}_e = 0$ and $\tilde{A}$ reduces to the familiar A matrix. However, for real gases, if we postmultiply A given by Eq. (7) by the vector $\bar{Q}$, we find that

$$A\bar{Q} = \bar{F} - \frac{e}{\rho}\tilde{\gamma}_\tau \begin{bmatrix} 0 \\ \rho \\ \rho u \end{bmatrix} \tag{9}$$

Thus, unless the derivative $\tilde{\gamma}_\tau = 0$, the Euler equations will not be homogeneous of degree one. This condition on the homogeneity of the Euler equations is consistent with the development in Ref. 2. This property, $\bar{F} = A\bar{Q}$, is utilized in the Steger-Warming[2] flux-split scheme.

We can proceed to develop real gas versions of these schemes by noting that the first term of Eq. (7), which reduces to the matrix A for a perfect gas, has the property

$$\tilde{A}\bar{Q} = \bar{F} \tag{10}$$

Note that, in general, $\tilde{A} \neq \partial\bar{F}/\partial\bar{Q}$, indicating that the splittings developed utilizing Eq. (10) will be approximate.

Steger-Warming Flux-Vector Splitting

We can develop an approximate flux splitting for real gases following Steger and Warming[2] by diagonalizing $\tilde{A}$ as

$$\tilde{\Lambda} = \tilde{S}^{-1}\tilde{A}\tilde{S} \tag{11}$$

where $\tilde{\Lambda}$ is a diagonal matrix whose elements are composed of the eigenvalues of $\tilde{A}$, which are

$$\tilde{\Lambda} = \begin{bmatrix} u & 0 & 0 \\ 0 & u + \tilde{a} & 0 \\ 0 & 0 & u - \tilde{a} \end{bmatrix} \tag{12}$$

where

$$\tilde{a}^2 \equiv \tilde{\gamma}p\tau \tag{13}$$

Note that $\tilde{a}$ is not the true speed of sound as given by Eq. (4). The quantity $\tilde{\gamma}$ is not a ratio of specific heats, but is found from τ, e, and p, Eq. (6) as

$$\tilde{\gamma} = \frac{\tau p(\tau, e)}{e} + 1 \tag{14}$$

The columns of the matrix $\tilde{S}$ consist of the right eigenvectors of $\tilde{A}$ as

$$\tilde{S} = \begin{bmatrix} 1 & 1 & 1 \\ u & u + \tilde{a} & u - \tilde{a} \\ u^2/2 & \tilde{H} + u\tilde{a} & \tilde{H} - u\tilde{a} \end{bmatrix} \tag{15}$$

where the quantity $\tilde{H}$, which reduces to the stagnation enthalpy for perfect gases, is defined as

$$\tilde{H} \equiv \frac{\tilde{a}^2}{\tilde{\gamma} - 1} + \frac{u^2}{2}$$

Now, a flux splitting may be developed by splitting $\tilde{\Lambda}$ into a non-negative matrix $\tilde{\Lambda}^+$ and a non-positive matrix $\tilde{\Lambda}^-$.

$$\tilde{\Lambda} = \tilde{\Lambda}^+ + \tilde{\Lambda}^- \tag{16}$$

Then, we may write the flux as

$$\bar{F} = \tilde{A}\bar{Q} = \tilde{S}\tilde{\Lambda}\tilde{S}^{-1}\bar{Q} = \tilde{S}(\tilde{\Lambda}^+ + \tilde{\Lambda}^-)\tilde{S}^{-1}\bar{Q}$$

$$= \tilde{A}^+\bar{Q} + \tilde{A}^-\bar{Q} = \bar{F}^+ + \bar{F}^- \tag{17}$$

The split fluxes $\bar{F}^\pm$ are directly found for this case as

$$\bar{F}^\pm = \frac{\rho}{2\tilde{\gamma}}\left\{ 2(\tilde{\gamma} - 1)\begin{bmatrix} 1 \\ u \\ u^2/2 \end{bmatrix}\lambda_1^+ + \begin{bmatrix} 1 \\ u + \tilde{a} \\ \tilde{H} + u\tilde{a} \end{bmatrix}\lambda_2^+ + \begin{bmatrix} 1 \\ u - \tilde{a} \\ \tilde{H} - u\tilde{a} \end{bmatrix}\lambda_3^+ \right\} \tag{18}$$

where

$$\lambda_1 = u, \quad \lambda_2 = u + \tilde{a}, \quad \lambda_3 = u - \tilde{a} \quad \lambda_i^+ = \tfrac{1}{2}[\lambda_i \pm |\lambda_i|]$$

$$i = 1,\ldots,3 \tag{19}$$

The scheme is then implemented by using upwind (relative to signal propagation speeds of $\lambda_i^\pm$) derivatives for the spatial derivatives of $\bar{F}^\pm$.

This approach may be observed to be an equivalent γ perfect gas formulation. Indeed, it may be implemented by using an equation of state $p = p(\rho, e)$ for the pressure, determining $\tilde{\gamma}$ with Eq. (14), and $\tilde{a}^2$ from Eq. (13). The preceding analysis shows which equivalent $\tilde{\gamma}$ to use. (Other forms that have been

utilized elsewhere include

$$\Gamma = a^2/p\tau$$

where a^2 is the true speed of sound obtained from Eq. (4) and not $\tilde{a}^2$ as used here.) Note that in the present approach, the fluxes are split according to the signs of $u \pm \tilde{a}$ and not $u \pm a$.

Van Leer Flux-Vector Splitting

The same procedure can be carried over to the Van Leer flux splitting.[3] This scheme has continuously differentiable flux contributions and has been shown to result in smoother solutions near sonic points.[6] The procedures of Ref. 3 may be extended to real gases by noting that we may write $\bar{F}$ as

$$\bar{F}(\rho,\tilde{a},\tilde{M}) = \begin{bmatrix} \rho\tilde{a}\tilde{M} \\ \rho\tilde{a}^2(\tilde{M}^2 + 1/\tilde{\gamma}) \\ \rho\tilde{a}^3\tilde{M}\left[\dfrac{\tilde{M}^2}{2} + \dfrac{1}{(\tilde{\gamma}-1)}\right] \end{bmatrix} \tag{20}$$

where $\tilde{a}$ is the "equivalent speed of sound" given by Eq. (13), $\tilde{\gamma} = \tilde{\gamma}(e,\tau)$ given by Eq. (14), and the "equivalent Mach number" $\tilde{M}$ as

$$\tilde{M} = u/\tilde{a} \tag{21}$$

The flux splitting based on $\tilde{A}$ rather than A then becomes

$$\bar{F}^{\pm} = \begin{bmatrix} f_1^{\pm} \\ f_2^{\pm} \\ f_3^{\pm} \end{bmatrix} = \begin{bmatrix} \pm\rho\tilde{a}(\tilde{M} \pm 1)^2/4 \\ f_1^{\pm}[(\tilde{\gamma}-1)u \pm 2\tilde{a}]/\tilde{\gamma} \\ f_1^{\pm}[(\tilde{\gamma}-1)u \pm 2\tilde{a}]^2/2(\tilde{\gamma}^2-1) \end{bmatrix} \tag{22}$$

Note that if the flux-vector $\bar{F}$ were written in terms of the true Mach number and speed of sound, then

$$\bar{F}(\rho,a,M) = \begin{bmatrix} \rho aM \\ \rho a^2(M^2 + 1/\Gamma) \\ \rho a^3 M\left[\dfrac{M^2}{2} + \dfrac{\tilde{\gamma}}{\Gamma(\tilde{\gamma}-1)}\right] \end{bmatrix} \tag{23}$$

where $\tilde{\gamma}$ is defined by Eq. (14) and $\Gamma(p,\tau) = a^2/p\tau$. The procedures of Ref. 3 will not work directly for Eq. (23) because of the mixed γ appearing in the energy flux.

Flux-Difference Splitting—Roe

The essence of flux-difference splitting techniques is the solution of local Riemann problems stemming from the consideration of piecewise uniform states between cell interfaces on an initial data line. This procedure follows the spirit of Godunov's early development and has been considerably advanced by a number of researchers, as described in the survey papers of Refs. 1 and 4. Here we will follow the work of Roe.[4] In Roe's approach, the solution to an approximate Riemann problem is developed

$$\bar{Q}_t + \hat{A}\bar{Q}_x = 0 \tag{24}$$

where $\hat{A}$ is a (locally constant) matrix for each pair of initial data $(\bar{Q}_\ell, \bar{Q}_r)$. The requirements for $\hat{A}$ are described in Ref. 7 with the major property being

$$\Delta\bar{F} = \hat{A}\,\Delta\bar{Q} \tag{25}$$

where $\Delta\bar{Q} = \bar{Q}_r - \bar{Q}_\ell$ and $\Delta\bar{F} = \bar{F}_r - \bar{F}_\ell$. A straightforward procedure for generating $\hat{A}$ is given for the case of a perfect gas in terms of parameter vectors.[7] We follow this procedure for a real gas by introducing the parameter vector (shown here in one space dimension) as

$$\bar{W} = \rho^{1/2}\begin{bmatrix} 1 \\ u \\ H \end{bmatrix} \tag{26}$$

For a perfect gas, both $\bar{Q}$ and $\bar{F}$ are quadratic in terms of the components of $\bar{W}$. For a real gas, this will not be true because of the equation of state for $p = p(e,\tau)$. This feature may be more clearly elucidated by again introducing an equivalent $\tilde{\gamma}$ [as in Eq. (6)], which in terms of these variables

$$\begin{aligned} p &= \frac{\tilde{\gamma}-1}{\tilde{\gamma}}(\rho H - \rho u^2/2) \\ &= \frac{\tilde{\gamma}-1}{\tilde{\gamma}}(w_1 w_3 - w_2^2/2) \end{aligned} \tag{27}$$

We see that

$$\begin{bmatrix} q_1 \\ q_2 \\ q_3 \end{bmatrix} = \begin{bmatrix} w_1^2 \\ w_1 w_2 \\ w_1 w_3 - p \end{bmatrix}, \qquad \begin{bmatrix} f_1 \\ f_2 \\ f_3 \end{bmatrix} = \begin{bmatrix} w_1 w_2 \\ w_2^2 + p \\ w_2 w_3 \end{bmatrix} \tag{28}$$

The presence of $\tilde{\gamma}(e,\tau)$ in the pressure term Eq. (27) will complicate the use of the parameter vector $\bar{W}$ as seen in Eq. (28). We wish to find a matrix $\hat{B}$ such that

$$\Delta\bar{Q} = \hat{B}\,\Delta\bar{W} \tag{29}$$

and a $\hat{C}$ such that

$$\Delta\bar{F} = \hat{C}\,\Delta\bar{W} \tag{30}$$

and then eliminate $\Delta\bar{W}$ to determine a matrix $\hat{A}$ where $\Delta\bar{F} = \hat{A}\,\Delta\bar{Q}$:

$$\hat{A} = \hat{C}\hat{B}^{-1} \tag{31}$$

In order to find $\hat{B}$ and $\hat{C}$, we need the jumps in the quadratic w terms in Eqs. (28) along with Δp from Eq. (27). The jump Δp is complicated by nonuniqueness associated with jumps involving more than two terms (discussed by Roe[7]) and because the jump will involve $\Delta\tilde{\gamma}$, which is not readily available in terms of Δw. We may, however, take advantage of the fact that across any cell interfaces the jumps in $\tilde{\gamma}$ will always be relatively small. Then

$$\begin{aligned} \Delta p = &\left\langle\left(\frac{\tilde{\gamma}-1}{\tilde{\gamma}}\right)\right\rangle(\hat{w}_3\Delta w_1 - \hat{w}_2\Delta w_2 + \hat{w}_1\Delta w_3) \\ &+ \langle w_1 w_3 - w_2^2/2\rangle\Delta\left(\frac{\tilde{\gamma}-1}{\tilde{\gamma}}\right) \end{aligned} \tag{32}$$

The Δf terms represent the jumps $f_r - f_\ell$, and the $\langle f\rangle$ terms are used to represent the arithmetic mean value $(1/2)(f_r + f_\ell)$. The $\hat{w}$ terms also are used to represent $\langle w\rangle$. It can be shown that

$$\left\langle\frac{\tilde{\gamma}-1}{\tilde{\gamma}}\right\rangle = \frac{\hat{\gamma}-1}{\hat{\gamma}} + 0(\Delta\tilde{\gamma})^2$$

$$\Delta\left\langle\frac{\tilde{\gamma}-1}{\tilde{\gamma}}\right\rangle = \frac{\Delta\tilde{\gamma}}{\hat{\gamma}^2} + 0(\Delta\tilde{\gamma})^3$$

and

$$\left\langle w_1 w_3 - \frac{w_2^2}{2}\right\rangle = \left(\frac{\hat{\gamma}}{\hat{\gamma}-1}\right)\hat{p} - \frac{1}{4}\frac{\Delta p\Delta\tilde{\gamma}}{(\hat{\gamma}-1)^2} + 0(\Delta\tilde{\gamma})^2$$

where $\hat{\gamma} \equiv \langle \tilde{\gamma} \rangle$. Thus, we can express Δp as

$$\Delta p = \left(\frac{\hat{\gamma}-1}{\hat{\gamma}}\right)(\hat{w}_3\Delta w_1 - \hat{w}_2\Delta w_2 + \hat{w}_1\Delta w_3) + \frac{1}{\hat{\gamma}(\hat{\gamma}-1)}\hat{p}\Delta\tilde{\gamma} + 0(\Delta\tilde{\gamma})^2 \tag{33}$$

In order to complete the formulation of $\Delta\bar{Q}$ and $\Delta\bar{F}$ in terms of ΔW, we need at least an approximation to $\Delta\tilde{\gamma}$. An interesting approach to this problem is found in Colella and Glaz[5] where they developed a differential equation for $\tilde{\gamma}$ valid for isentropic flow. This equation may be derived starting from Eq. (6) whereby

$$d\tilde{\gamma} = \frac{\tau}{e}\,dp + \frac{p}{e}\,d\tau - \frac{p\tau}{e^2}\,de$$

The first law of thermodynamics gives for an isentropic flow $de = p\,d\tau$, and we may utilize $a^2 = -\tau^2\,dp/d\tau$ (for an isentropic flow) so that

$$d\tilde{\gamma} = (\tilde{\gamma}-1)\left(1 - \frac{\tilde{\gamma}p\tau}{a^2}\right)\frac{dp}{p}$$

and if we define

$$\Gamma \equiv a^2/p\tau \tag{34}$$

then

$$d\tilde{\gamma} = (\tilde{\gamma}-1)\left[1 - \frac{\tilde{\gamma}}{\Gamma}\right]\frac{dp}{p} \tag{35}$$

Equation (35) is strictly valid only for an isentropic flow. The function $\Gamma = \Gamma(e,\tau)$, since the real-gas equation of state will give $p = p(e,\tau)$ and $a = a(e,\tau)$ [from Eq. (4)].

Since the jumps in $\tilde{\gamma}$ and Γ are assumed to be very small, Eq. (35) may be approximated as

$$\Delta\tilde{\gamma} \approx (\hat{\gamma}-1)\left[1 - \frac{\hat{\gamma}}{\hat{\Gamma}}\right]\frac{\Delta p}{\hat{p}} \tag{36}$$

The specific averaging process used for $\hat{\gamma}$ and $\hat{\Gamma}$ are not important here, since we are assuming small values for $\Delta\tilde{\gamma}$ and $\Delta\Gamma$. Substituting Eq. (36) into Eq. (33) we obtain

$$\Delta p\left[1 - \left(1 - \frac{\hat{\gamma}}{\hat{\Gamma}}\right)\frac{1}{\hat{\gamma}}\right] = \left(\frac{\hat{\gamma}-1}{\hat{\gamma}}\right) \times (\hat{w}_3\Delta w_1 - \hat{w}_2\Delta w_2 + \hat{w}_1\Delta w_3) \tag{37}$$

We further assume that $\hat{\gamma}$ is nearly equal to $\hat{\Gamma}$ (a very reasonable physical assumption) such that a small term ϵ may be introduced

$$\epsilon \equiv \left(\frac{\hat{\gamma}}{\hat{\Gamma}} - 1\right)\frac{1}{\hat{\gamma}} \tag{38}$$

so that

$$\Delta p \approx \frac{(\hat{\gamma}-1)}{\hat{\gamma}}(1-\epsilon)(\hat{w}_3\Delta w_1 - \hat{w}_2\Delta w_2 + \hat{w}_1\Delta w_3) \tag{39}$$

Now, utilizing Eq. (39) and Eq. (28), we may evaluate $\hat{B}$ defined in Eq. (29) and $\hat{C}$ defined in Eq. (30) as

$$\hat{B} = \frac{1}{\langle\rho^{1/2}\rangle} \times \begin{bmatrix} 2 & 0 & 0 \\ \hat{u} & 1 & 0 \\ \left[\dfrac{1+\epsilon(\hat{\gamma}1)}{\hat{\gamma}}\right]\hat{H} & \dfrac{(\hat{\gamma}-1)(1-\epsilon)}{\hat{\gamma}}\hat{u} & \dfrac{1+\epsilon(\hat{\gamma}-1)}{\hat{\gamma}} \end{bmatrix} \tag{40}$$

and

$$\hat{C} = \frac{1}{\langle\rho^{1/2}\rangle} \times \begin{bmatrix} \hat{u} & 1 & 0 \\ \dfrac{(\hat{\gamma}-1)(1-\epsilon)\hat{H}}{\hat{\gamma}} & \left[\dfrac{(\hat{\gamma}+1)+\epsilon(\hat{\gamma}-1)}{\hat{\gamma}}\right]\hat{u} & \dfrac{(\hat{\gamma}-1)(1-\epsilon)}{\hat{\gamma}} \\ 0 & \hat{H} & \hat{u} \end{bmatrix} \tag{41}$$

The quantities $\hat{u}$ and $\hat{H}$ above are defined as

$$\hat{u} \equiv \frac{\hat{w}_2}{\hat{w}_1} = \frac{\langle\rho^{1/2}u\rangle}{\langle\rho^{1/2}\rangle} \tag{42}$$

and

$$\hat{H} \equiv \frac{\hat{w}_3}{\hat{w}_1} = \frac{\langle\rho^{1/2}H\rangle}{\langle\rho^{1/2}\rangle} \tag{43}$$

We then determine

$$\hat{A} = \begin{bmatrix} 0 & 1 & 0 \\ [\hat{\gamma}-3-\epsilon\hat{\gamma}(\hat{\gamma}-1)]\dfrac{\hat{u}^2}{2} & [3-\hat{\gamma}+\epsilon\hat{\gamma}(\hat{\gamma}-1)]\hat{u} & (\hat{\gamma}-1)(1-\epsilon\hat{\gamma}) \\ (\hat{\gamma}-1)(1-\epsilon\hat{\gamma})\dfrac{\hat{u}^3}{2} - \hat{H}\hat{u} & \hat{H} - (\hat{\gamma}-1)(1-\epsilon\hat{\gamma})\hat{u}^2 & [1-\epsilon(\hat{\gamma}-1)]\hat{\gamma}\hat{u} \end{bmatrix} \tag{44}$$

The eigenvalues of $\hat{A}$ are found to be

$$\lambda_1 = \hat{u}, \qquad \lambda_2 = \hat{u} + \hat{a}, \qquad \lambda_3 = \hat{u} - \hat{a} \tag{45}$$

and the corresponding eigenvectors

$$\hat{e}_1 = \begin{bmatrix} 1 \\ \hat{u} \\ \hat{u}^2/2 \end{bmatrix}, \quad \hat{e}_2 = \begin{bmatrix} 1 \\ \hat{u}+\hat{a} \\ \hat{H}+\hat{u}\hat{a} \end{bmatrix}, \quad \hat{e}_3 = \begin{bmatrix} 1 \\ \hat{u}-\hat{a} \\ \hat{H}-\hat{u}\hat{a} \end{bmatrix} \tag{46}$$

where $\hat{u}$ and $\hat{H}$ are previously defined and with Eq. (28)

$$\hat{a}^2 \equiv (\hat{\gamma}-1)(1-\hat{\gamma}\epsilon)(\hat{H} - \hat{u}^2/2) = \frac{(\hat{\gamma}-1)\hat{\Gamma}}{\hat{\gamma}}(\hat{H} - \hat{u}^2/2) \tag{47}$$

We see that for the case of a perfect gas where $\hat{\gamma} = \hat{\Gamma} = \gamma$, the original formulation of Roe is obtained.

The next step of applying Roe's procedure in developing the solution to the approximate Riemann problem consists of projecting $\Delta\bar{F}$ onto the eigenvectors of $\hat{A}$ such that

$$\Delta\bar{F} = \sum_{j=1}^{3} \lambda_j\alpha_j\bar{e}_j \tag{48}$$

where α_j are the strength of each wave traveling at wave speed λ_j. The α_j may be formally found by diagonalizing $\hat{A}$

$$\Delta\bar{F} = \hat{A}\,\Delta\bar{Q} = \hat{S}\hat{\Lambda}\hat{S}^{-1}\,\Delta\bar{Q} \tag{49}$$

where the columns of $\hat{S}$ are the right eigenvectors of $\hat{A}$, and $\hat{\Lambda}$ is a diagonal matrix composed of the eigenvalues of $\hat{A}$. Then,

$(\alpha_1\ \alpha_2\ \alpha_3)^T = \hat{S}^{-1}\Delta\bar{Q}$, and we find that

$$\alpha_1 = \left[1 - \frac{\hat{\Gamma}(\hat{\gamma}-1)}{2\hat{\gamma}}\frac{\hat{u}^2}{\hat{a}^2}\right]\Delta\rho + \frac{\hat{\Gamma}(\hat{\gamma}-1)}{\hat{\gamma}}\frac{\hat{u}}{\hat{a}^2}\Delta(\rho u) \tag{50a}$$

$$\alpha_{2,3} = \mp\frac{\hat{u}}{2\hat{a}}\left[1 \pm \frac{\hat{\Gamma}(\hat{\gamma}-1)}{2\hat{\gamma}}\frac{\hat{u}}{\hat{a}}\right]\Delta\rho \pm \frac{1}{2\hat{a}}\left[1 \pm \frac{\hat{\Gamma}(\hat{\gamma}-1)}{\hat{\gamma}}\frac{\hat{u}}{\hat{a}}\right]\Delta(\rho u) + \frac{\hat{\Gamma}(\hat{\gamma}-1)}{2\hat{\gamma}\hat{a}^2}\Delta(\rho E) \tag{50b}$$

Alternately, we may recombine the jumps in the elements of $\Delta\bar{Q}$ in Eq. (50) into jumps in Δp, $\Delta\rho$, and Δu using Eq. (37) as

$$\alpha_1 = (1/\hat{a}^2)[\hat{a}^2\Delta\rho - \Delta p] \tag{51a}$$

$$\alpha_{2,3} = (1/2\hat{a}^2)[\Delta p \pm \hat{\rho}\hat{a}\Delta u] \tag{51b}$$

where $\hat{\rho} = (\rho_\ell \rho_r)^{1/2}$. The above form of wave strengths corresponds to the original development of Roe's method, but the appropriate "averaging" of $\hat{a}$ for a real gas [Eq. (47)] must be used. The interface fluxes used in algorithm are then computed from

$$\bar{F}_{i+1/2}(\bar{Q}_\ell, \bar{Q}_r) = \frac{1}{2}\left[\bar{F}_\ell + \bar{F}_r - \sum_{j=1}^{3} |\lambda_j|\alpha_j\bar{e}_j\right] \tag{52}$$

Applications

The first illustration of this method is for a one-dimensional unsteady flow computation using the Steger-Warming flux splitting, as developed for real gases in Eqs. (18) and (19). We have chosen a shock-tube problem with a very high temperature and high-pressure driver section. The conditions used are for the driver:

$p_4 = 100$ atm
$T_4 = 9000$ K
$\rho_4 = 2.641$ kg/m^3
$e_4 = 5216$ Kcal/kg

and for the driven

$p_1 = 1$ atm
$T_1 = 300$ K
$\rho_1 = 1.174$ kg/m^3
$e_1 = 51.33$ Kcal/kg

The gas is equilibrium air. We have used the simplified curve fits of Ref. 8 for the calculation, both finite difference and exact. The exact computation is nontrivial and involves iterative procedures for the shock and numerical quadratures for the centered expansion. A discussion of the exact shock-tube solution for real gases may be found in Ref. 5.

We utilized a second-order-accurate in space and time-numerical algorithm for the finite-difference solution to this problem. Spatial differences were developed with a MUSCL differencing approach, as discussed in Ref. 6. The two-step algorithm may be written as

$$\tilde{Q}_i = Q_i^n - \frac{\Delta t}{\Delta x}[F^+(Q_{i+1/2}^-) - F^+(Q_{i-1/2}^-)] - \frac{\Delta t}{\Delta x}[F^-(Q_{i+1/2}^+) - F^-(Q_{i-1/2}^+)]$$

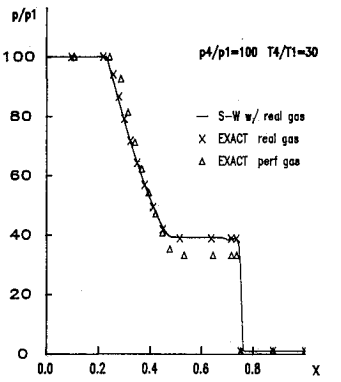

a) Shock-tube problem—pressure distribution

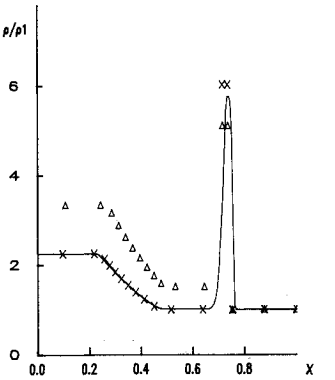

b) Shock-tube problem—density distribution

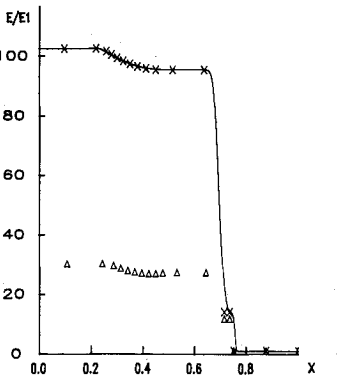

c) Shock-tube problem—total energy distribution

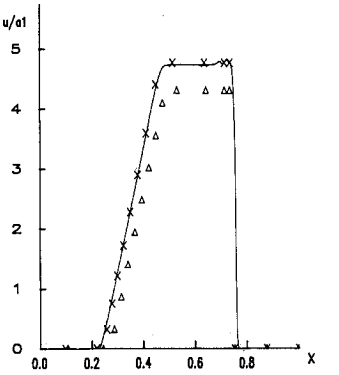

d) Shock-tube problem—velocity distribution

Fig. 1 Shock-tube problem. Numerical solution with Steger-Warming flux-vector splitting for equilibrium air.

and

$$Q_i^{n+1} = \frac{1}{2}\{Q_i^n + \tilde{Q}_i - \frac{\Delta t}{\Delta x}[F^+(\tilde{Q}^-_{i+\frac{1}{2}}) - F^+(\tilde{Q}^-_{i-\frac{1}{2}})]$$

$$- \frac{\Delta t}{\Delta x}[F^-(\tilde{Q}^+_{i+\frac{1}{2}}) - F^-(\tilde{Q}^+_{i-\frac{1}{2}})]\}$$

where the split fluxes $F^{\pm}$ are given in Eq. (19), and for second-order spatial accuracy

$$Q^-_{i+\frac{1}{2}} = Q_i + \tfrac{1}{2}(Q_i - Q_{i-1})$$

$$Q^+_{i+\frac{1}{2}} = Q_{i+1} + \tfrac{1}{2}(Q_{i+1} - Q_{i+2})$$

We applied this MUSCL extrapolation to ρ, ρu, and also to the pressure p as determined from the equilibrium flow tables and $\tilde{\gamma}$ from Eq. (14). The flux $(\rho E)^{\pm}_{i+\frac{1}{2}}$ was found from p, ρ, ρu, and $\tilde{\gamma}$. We also incorporated a flux limiter, the so-called min-mod limiter.[6,9]

We computed the shock-tube problem with 180 mesh points in the x-direction and 162 time steps with the shock moving from $x = 0.50$ to approximately $x = 0.75$. The numerical calculation using the Steger-Warming splitting labeled *S-W* along with exact perfect and real gas solutions are shown in Fig. 1 for the quantities p/p_1, ρ/ρ_1, E/E_1, and u/a_1. The results are generally in excellent agreement with the exact real-gas solution. The shocks are captured very sharply with some slight smearing across the contact surface. The problem has an exceptional strong jump across the contact, as seen in the density and energy plots.

Implementation of equilibrium air properties into an existing two-dimensional flux-vector split (FVS) perfect gas Euler code is a straightforward extension of the one-dimensional case. The cell-centered finite-volume code, as described in Ref. 10, utilizes the Van Leer flux splittings.

The flux vectors (unsplit and split) for the equilibrium air code were obtained by replacing the pressure calculated from a perfect gas equation of state with the pressure determined by an equilibrium air curve fit $p = p(\rho,e)$, using the code described in Ref. 7, and the constant ratio of specific heats γ was replaced by the equivalent $\tilde{\gamma}(\rho,e)$ given by Eq. (14). The Jacobian matrices associated with the linearization of the flux vectors are likewise altered.

In order to obtain values of the conserved variables $\bar{Q} = [\rho, \rho u, \rho v, \rho E]^T$ at a cell face for the flux calculations, the variable $\bar{Q}_e = [\rho, \rho u, \rho v, p, \tilde{\gamma}]^T$ was extrapolated from cell centers to cell faces by use of

$$[Q_e^-]_{i+\frac{1}{2},j} = \left\{I + \frac{s_{ij}}{4}[(1 - \kappa s_{i,j})\nabla + (1 + \kappa s_{i,j})\Delta]\right\} Q_{e_{i,j}}$$

$$[Q_e^+]_{i+\frac{1}{2},j} = \left\{I - \frac{s_{i+1,j}}{4}[(1 + \kappa s_{i+1,j})\nabla + (1 - \kappa s_{i+1,j})\Delta]\right\} Q_{e_{i+1,j}}$$

where

$$\Delta Q_{e_{i,j}} = Q_{e_{i+1,j}} - Q_{e_{i,j}}$$

$$\nabla Q_{e_{i,j}} = Q_{e_{i,j}} - Q_{e_{i-1,j}}$$

and κ controls the spatial accuracy ($\kappa = -1$ for a fully upwind, second-order scheme). The term $s_{i,j}$ is a limiter, determined from

$$s_{i,j} = \left[\frac{2\nabla Q_e \Delta \bar{Q}_e + \epsilon}{(\Delta Q_e)^2 + (\nabla Q_e)^2 + \epsilon}\right]_{i,j}$$

and $\epsilon = 10^{-6}$. Having computed the cell-face values $\bar{Q}_e$, the total energy is calculated from

$$\rho E = \frac{p}{\tilde{\gamma} - 1} + \frac{\rho(u^2 + v^2)}{2}$$

All of the cell-face values of the conserved variables are known and, hence, the split-flux contributions can be determined. The splitting in the ξ-direction is based on the testing of the equivalent Mach number

$$\tilde{M}_\xi = \tilde{u}/\tilde{a}$$

where $\tilde{u}$ is the velocity component at the cell face normal to a line of constant ξ, and $\tilde{a}$ is the equivalent speed of sound defined by Eq. (13). Similar formulas hold in the η-direction.

As an initial two-dimensional test case, a high-temperature internal flow through a simple inlet was considered. The inlet consisted of a 10 deg wedge followed by a 10 deg expansion and is symmetric about the centerline. The 201 × 51 grid was uniformly spaced in the x-direction and slightly clustered near the wall in the y-direction. At the inflow boundary, all conditions were held constant at the reference conditions of $T_\infty = 3573$ K, $p_\infty = 101{,}325$ N/m^2, $\rho_\infty = 0.0883$ kg/m^3, and $M_\infty = 5.0$. The outflow boundary is supersonic; therefore, no conditions are specified there. On the surface, wall tangency was enforced along with imposing that the wall enthalpy,

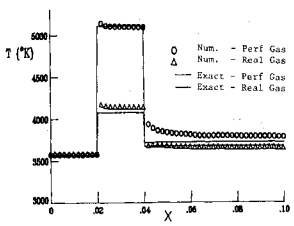

a) Surface temperature distribution

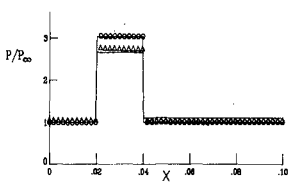

b) Surface pressure distribution

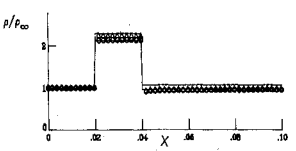

c) Surface density distribution

Fig. 2 Supersonic wedge problem. Freestream conditions: $M_\infty = 5$, $T_\infty = 3573$ K, $p_\infty = 101{,}325$ N/m^2, $\rho_\infty = 0.0883$ kg/m^3. Numerical solutions with Van Leer flux-vector splitting for equilibrium air and perfect gas.

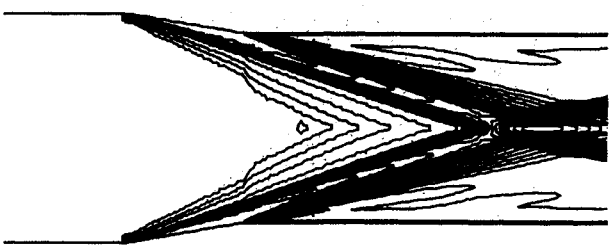

Fig. 3 Supersonic wedge problem. Equilibrium air temperature contours.

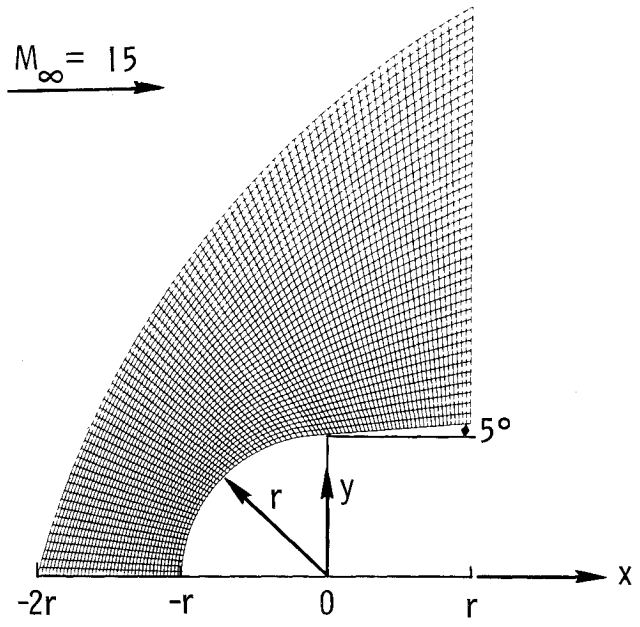

Fig. 4 Hypersonic blunt-body problem. Grid distribution on a 41 × 81 mesh.

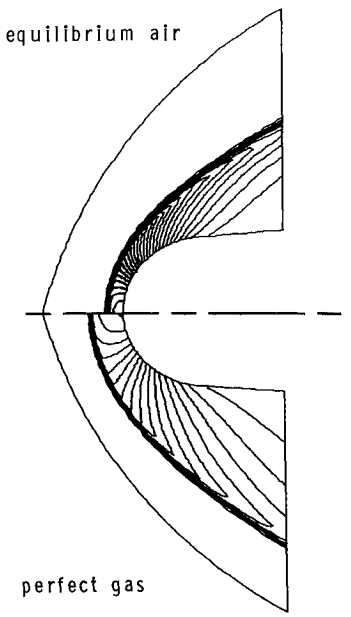

Fig. 5 Hypersonic blunt-body problem. Pressure contour comparison for equilibrium and perfect gas. Freestream conditions: $M_\infty = 15$, $T_\infty = 295$ K, $p_\infty = 170$ N/m^2, $\rho_\infty = 0.002$ kg/m^3. Numerical solutions with Roe's flux-difference splitting.

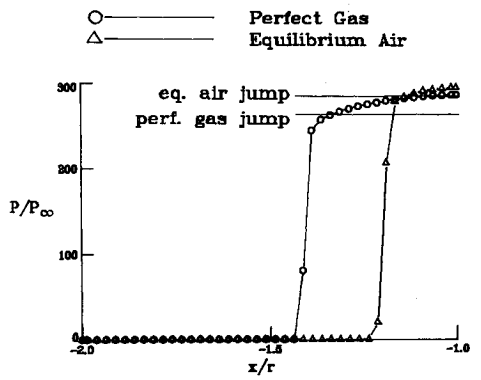

a) Hypersonic blunt-body problem—surface pressure distribution

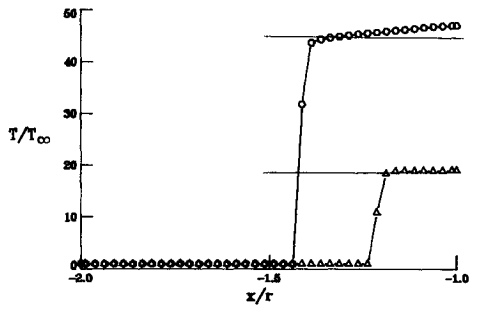

b) Hypersonic blunt-body problem—surface temperature distribution

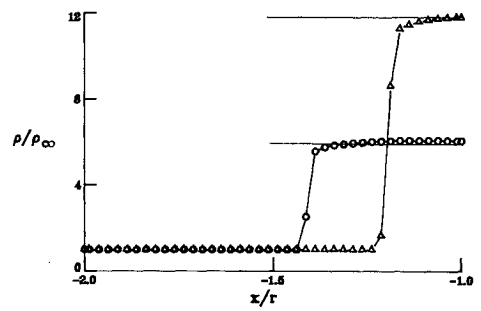

c) Hypersonic blunt-body problem—surface density distribution

Fig. 6 Hypersonic blunt-body problem, surface distribution comparisons. Numerical solutions with Roe's flux-difference splitting.

entropy, and pressure are equal to the values at the first cell center off of the wall. Symmetry conditions were used on the grid centerline. Figure 2 compares numerical and theoretical predictions for temperature, pressure, and density distributions for both perfect gas and equilibrium air equations of state. Obviously, a major discrepancy exists in the temperature prediction between the perfect and equilibrium air models. Temperature contours are also plotted in Fig. 3 to give an indication of the geometry.

The algorithm used to solve the governing equations is a vectorized version of vertical line Gauss-Seidel, written for the CYBER-205 at NASA Langley. The CPU time per iteration per mesh point of the perfect gas version is 58 μs/iter/mp, whereas the real gas version runs at 96 μs/iter/mp. However, the equilibrium air pressure calculation is presently being done with a scalar routine. It is expected that the vectorized version will significantly reduce the differences that exist between the perfect and real gas CPU times. For both codes, the CPU time/iteration can be reduced roughly by half by saving and reusing the LU decomposition.

Another test case considered was the Mach 15 flow over the blunt body shown in Fig. 4. As indicated in the figure, a relatively course 41 × 81 grid was used for this calculation. Reference conditions were chosen to correspond to atmospheric conditions at an altitude of 45 km: $p = 170$ N/m^2, $\rho = 0.002$ kg/m^3, $T = 295$ K. For this case, solutions were generated using both perfect gas and equilibrium air versions of Roe's flux-difference splitting (FDS) approach. A comparison of pressure contours between the perfect gas and equilibrium air solutions using FDS is shown in Fig. 5. Major differences may be seen to exist in the contour plots, especially with respect to shock standoff distance. Figure 6 compares the distribution of pressure, temperature, and density on the symmetry line. In addition, the exact solution for a normal shock has been indicated on these figures, using both perfect gas and equilibrium air equations of state, since on the symmetry line the bow shock is effectively normal. Finally, Fig. 7 contains plots of pressure, temperature, and density on the surface of

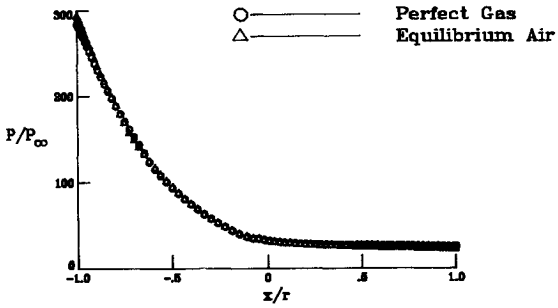

a) Hypersonic blunt-body problem—pressure distribution along symmetry line

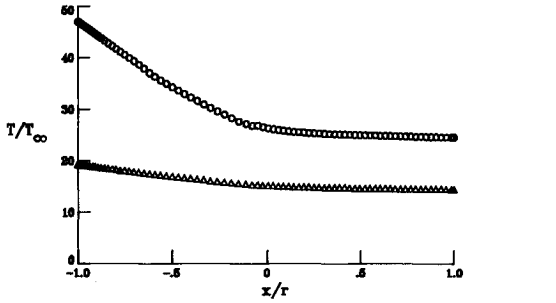

b) Hypersonic blunt-body problem—temperature distribution along symmetry line

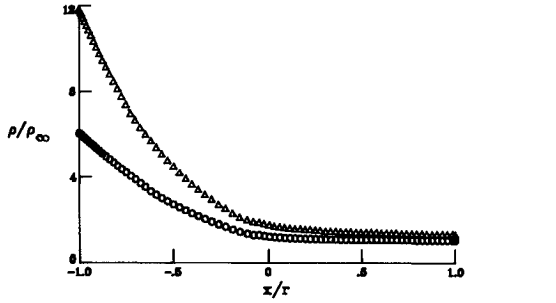

c) Hypersonic blunt-body problem—density distribution along symmetry line

Fig. 7 Hypersonic blunt-body problem, symmetry line comparisons. Numerical solutions with Roe's flux-difference splitting.

the body. The perfect gas and equilibrium air surface pressure distributions essentially coincide, whereas there are very significant differences in the temperature and density distributions, especially in the stagnation region.

Concluding Remarks

A new set of flux-splitting procedures have been developed for real gas flow computations. The approach, which takes the form of an equivalent γ representation, approximately accounts for real gas effects in the structure of the flux-split algorithms. The methods may be easily included into existing perfect gas codes incorporating the Steger-Warming and Van Leer flux-vector splittings and the Roe flux-difference splitting. Results presented here show excellent agreement with exact solutions for the high-temperature flow of air in chemical equilibrium, in a shock tube, and over a wedge-shoulder configuration. More details of the method, particularly the implementation for three-dimensional flows along with more computational examples, appear in Ref. 11. Some new flux-split algorithms, which do not depend upon the approximations utilized here, have recently been developed by Vinokur and Liu[12] and Glaister.[13] These algorithms should, in principle, be more accurate than those presented here. However, they appear to be more complicated to implement and possibly computationally expensive. In addition, multidimensional solutions have not yet been presented with these methods.

Acknowledgment

This research was partially funded by the NASA Langley Research Center under Grants NAG-1-684 and NAG-1-776.

References

[1]Harten, A., Lax, P. D., and Van Leer, B., "On Upstream Differencing and Godunov-Type Schemes for Hyperbolic Conservation Laws," *SIAM Review,* Vol. 25, Jan. 1983, pp. 35–61.

[2]Steger, J. L. and Warming, R. F., "Flux Vector Splitting of the Inviscid Gasdynamic Equations with Application to Finite-Difference Methods," *Journal of Computational Physics,* Vol. 40, 1981, pp. 263–293.

[3]Van Leer, B., "Flux-Vector Splitting for the Euler Equations," ICASE Rept. 82-30. Sept. 1982; *Lecture Notes in Physics,* Vol. 170, Springer-Verlag, 1982, pp. 507–512.

[4]Roe, P. L., "Characteristic-Based Schemes for the Euler Equations," *Annual Review of Fluid Mechanics,* Vol. 18, 1986, pp. 337–365.

[5]Colella, P. and Glaz, P. M., "Efficient Solution Algorithms for the Riemann Problem for Real Gases," *Journal of Computational Physics,* Vol. 59, 1985, pp. 264–289.

[6]Anderson, W. K., Thomas, J. L., and Van Leer, B., "A Comparison of Finite-Volume Flux Vector Splittings for the Euler Equations," AIAA Paper 85-0122, Jan. 1985.

[7]Roe, P. L., "Approximate Riemann Solvers, Parameter Vectors, and Difference Schemes," *Journal of Computational Physics,* Vol. 43, 1981, pp. 357–372.

[8]Srinivasan, S., Tannehill, J. C., and Weilmuenster, K. J., "Simplified Curve Fits for the Thermodynamic Properties of Equilibrium Air," NASA Reference Publication 1181, Aug. 1987.

[9]Sweby, P. K., "High Resolution Schemes Using Flux Limiters for Hyperbolic Conservation Laws," *SIAM Journal of Numerical Analysis,* Vol. 21, No. 5, Oct. 1984. pp. 995–1011.

[10]Walters, R. W. and Dwoyer, D. L., "An Efficient Iteration Strategy Based on Upwind/Relaxation Schemes for the Euler Equations," AIAA Paper 85-1529-CP, July 1985.

[11]Grossman, B. and Walters, R. W., "Flux Split Algorithms for the Multidimensional Euler Equations with Real Gases," *Journal of Computers and Fluids* (to be published).

[12]Vinocur, M. and Liu, Y., "Equilibrium Gas Flow Computations II: An Analysis of Numerical Formulations of Conservation Laws," AIAA Paper 88-0127, Jan. 1988.

[13]Glaister, P., "An Approximate Linearised Riemann Solver for the Euler Equations for Real Gases," *Journal of Computational Physics,* Vol. 74, 1988, pp. 382–408.